Available online at www.sciencedirect.com

ScienceDirect

Developmental Biology 312 (2007) 448–460

DEVELOPMENTAL BIOLOGY

www.elsevier.com/developmentalbiology

# Prioritising guidance cues: Directional migration induced by substratum contours and electrical gradients is controlled by a rho/cdc42 switch

Ann M. Rajnicek *, Louise E. Foubister, Colin D. McCaig

*School of Medical Sciences, Institute of Medical Sciences, University of Aberdeen, Aberdeen AB25 2ZD, UK*

Received for publication 29 May 2007; revised 25 September 2007; accepted 25 September 2007
Available online 4 October 2007

**Abstract**

Coordinated cell migration is a fundamental feature of embryogenesis but the intracellular mechanism by which cells integrate co-existing extracellular cues to yield appropriate vectoral migration is unknown. Cells in the cornea are guided by a naturally occurring DC electric field (EF) (electrotaxis) as they navigate non-planar substrata but the relative potencies of electrotaxis and guidance by substratum shape (contact guidance) have never been determined. We tested the hypothesis that vectoral migration was controlled by selective activation of rac, cdc42 or rho in response to a 150 mV/mm EF or to a series of parallel substratum nanogrooves (NGs) 130 nm deep. EFs and NGs were presented singly or in combination. Electrotaxis of dissociated bovine corneal epithelial cells (CECs) on planar quartz required signalling by cdc42 and rho but not rac. Contact guidance by substratum NGs required rho but not cdc42 or rac activities. When an EF and NGs were superimposed in parallel, cathodal electrotaxis along NGs was enhanced compared to that on planar quartz but when they were superimposed orthogonally (vertical NGs with horizontal EF) cells were recruited from contact guidance to electrotaxis, suggesting that the EF was more potent. However, increasing the EF to 250 mV/mm was insufficient to recruit the majority to electrotaxis. Consistent for the cues in isolation, when an EF (150 mV/mm) and NGs were superimposed orthogonally, rac activity was not essential for either contact guidance or electrotaxis. However, attenuation of cdc42 signalling abolished electrotaxis and enhanced contact guidance relative to controls (no drug), whereas inhibiting rho signalling enhanced electrotaxis and rho stimulation enhanced contact guidance. Our data are consistent with the idea that migrating CECs use a cdc42/rho "switch" to sort vectoral cues, with cdc42 controlling electrotaxis and rho controlling contact guidance.


*Keywords:* Cornea; Epithelial cells; rho GTPases; Wound healing; Contact guidance; cdc42; rho; rac; Electrotaxis

## Introduction

Appropriately directed cell migration is critical for embryogenesis so understanding how cells detect and respond selectively to directional stimuli has widespread significance. This raises a fundamental question: how do cells sort, integrate or prioritise extracellular vectoral stimuli, especially those providing potentially conflicting cues? We explored the relative potency of corneal epithelial cell (CEC) contact guidance by substratum nanogrooves (NGs) and CEC electrotaxis by electric fields (EFs) since these cues co exist in the cornea.

The cornea of the terrestrial vertebrate eye consists of an epithelium with an underlying array of tightly packed, parallel collagen fibrils organised in ribbon-like lamellae with successive layers positioned at nearly right angles. This precise spatial order on the scale of nanometres (parallel collagen arrays) and micrometres (orthogonal lamellae) imparts structural integrity and transparency (Maurice, 1957). Corneal epithelial cells (CECs) migrate over this lattice as they reepithelialise wounds (Suzuki et al., 2003) so if substratum topography determines the direction of CEC migration (contact guidance), its geometry could facilitate (or hinder) reepithelialisation. This idea has been explored using artificial substrata etched with parallel micrometre scale grooves (microgrooves), which cause CECs to align or migrate parallel to the groove axis (Diehl et al., 2005; Teixeira et al., 2003; Dalton et al., 2001). There have been fewer studies of CEC alignment and migration on sub micrometre

* Corresponding author.
*E-mail address:* a.m.rajnicek@abdn.ac.uk (A.M. Rajnicek).

0012-1606/$ - see front matter © 2007 Elsevier Inc. All rights reserved.
doi:10.1016/j.ydbio.2007.09.051

topography, principally because of the technical challenges inherent in fabricating nanogrooves (NGs). Consequently, the ability of NGs to polarise CEC migration is equivocal (Diehl et al., 2005; Evans et al., 2005; Teixeira et al., 2004, 2003, 2006). Here we tested the ability of substratum grooves similar in scale to those encountered in situ (130 nm deep) to guide CEC migration.

In addition to substratum topography CECs reepithelialising the injured cornea encounter a steady DC electric field (EF). Polarised movement of ions across the tightly sealed epithelium ($Na^+$ from tear fluid to stroma and $Cl^-$ from stroma to tear fluid) results in a transepithelial potential (TEP) difference of ~40 mV (stroma positive) in the intact cornea (Song et al., 2004). Any breach of epithelial integrity, such as wounding, results in instantaneous collapse of the TEP at the wound site (0 mV) but the TEP is maintained at normal levels distally. Therefore, wounding establishes a lateral gradient of TEP within the corneal tissues and consequently, an EF parallel to the epithelium, with the wound as the cathode. EFs of 40 to 200 mV/mm (Barker et al., 1982; Sta Iglesia and Vanable, 1998) have been measured near mammalian skin wounds and a wound-induced EF of 42 mV/mm has been measured directly in bovine cornea, although the authors consider this an underestimate (Chiang et al., 1992). Pharmacological manipulation of the wound-induced EF in the rat cornea affects reepithelialisation such that reduction in the EF inhibits wound healing and augmentation of the EF speeds healing (Song et al., 2004; Reid et al., 2005; Zhao et al., 2006). Additionally, in vitro individual CECs, sheets of CECs and the leading edge of an organ culture model of corneal wounding migrate towards the cathode of a physiological EF (Farboud et al., 2000; Zhao et al., 2003, 2006), supporting the notion that the natural EF promotes healing.

Despite evidence that artificial NG substrata and EFs direct CEC migration independently, the consequence of their superimposition has never been tested directly. Multiple cues may yield unpredicted or complex behaviours. For example, fibroblasts or neuronal growth cones co-presented with orthogonally oriented substratum stripes of adhesive proteins and NGs or an orthogonal EF, crossed obstacles they would normally avoid (Britland and McCaig, 1996; Britland et al., 1996). Similarly, the presence of an extracellular fibrillar scaffold alters the threshold EF strength required to induce fibroblast migration (Sun et al., 2004). Here, we tested the relative contributions of an EF and substratum NGs on directional CEC migration using an in vitro assay that allows their precise spatial control. The vectoral cues were superimposed in parallel to test their ability to augment directional migration and they were superimposed orthogonally to establish a hierarchy of their relative contributions to directional migration.

Cell alignment by substratum grooves is determined by the size and spacing of substratum ridges, which dictate the surface area and orientation of focal contacts (den Braber et al., 1998; Walboomers et al., 1998) but the intracellular mechanisms that underpin directional migration by nanotopography are unknown. In contrast, some molecules that mediate cathodal electrotaxis of CECs have been identified (Zhao et al., 1999, 2006; McBain et al., 2003). Most are upstream of the rho GTPases cdc42 and rho, which control cytoskeletal dynamics spatially.

Here we tested the relative potency of NGs and EFs as directional cues for cell migration and determined the relative requirements for rac, rho, cdc42 and their effectors on guidance. Our data suggest that a cdc42/rho "switch" determines whether NGs or the EF is the dominant cue. It is likely therefore that a balance of cdc42 and rho activity controls cell directed CEC migration in the cornea. The results are also relevant to repair of intractable wounds, which may be facilitated by a bioengineering derived therapy incorporating aligned nanotopography, DC EFs and pharmacological manipulation of cdc42 and rho signals.

## Materials and methods

### *Grooved substrata and corneal cell culture*

Primary cultures of epithelial cells were prepared from the limbal region of adult bovine eyes using the modification of the method of Gipson and Grill (1982) described by Zhao et al. (1996b). Explants (3 mm × 3 mm) from the limbal region of the cornea were dissociated in 1.2 IU/ml dispase II (Boehringer Mannheim) for 2 h at 37 °C. The underlying stroma was discarded and the epithelial layer was dissociated in 0.25% trypsin (Gibco-BRL) for ~5 min at 37 °C with gentle shaking. Trypsin activity was inhibited by addition of 10% fetal bovine serum (FBS-Sigma) and the cell suspension was centrifuged at 1000 rpm at room temperature for ~10 min. The pellet was resuspended in Minimal Essential Medium (MEM) with Hank's salts supplemented with 10% FBS, 25 mM HEPES, amino acid supplement, 2.5 μg/ml fungizone, 100 IU/ml penicillin, 100 μg/ml streptomycin, 2 mM L-glutamine (all from Gibco-BRL), pH 7.3 and centrifuged as before. The final pellet was resuspended in MEM for plating. Substitution of HEPES buffer for bicarbonate in the medium permits cell growth in room air rather than a 5% $CO_2$ environment. Typically, two corneas were dissociated in a final volume of 6 ml medium. After 2 h at 37 °C the slides were examined for CEC attachment and the dish was flooded with medium. After 18 h, medium was exchanged for fresh medium, which sometimes contained a drug.

The corneal epithelial cell (CEC) suspension was plated onto custom made quartz microscope slides (Department of Electronics and Electrical Engineering, Glasgow University) etched using electron beam lithography to yield grooves 130 nm deep in three separate 5 mm × 5 mm regions on an ungrooved (flat) background. The grooved slides were identical to those used previously for neurons (Rajnicek et al., 1997). Grooves and ridges had equal widths (e.g. each groove was flanked by ridges of the same width as the groove and vice versa) and were parallel, with approximately vertical "walls". The groove and ridge widths in each region were 1, 2 or 4 μm, respectively. Therefore, each slide provides four topographies; (i) flat quartz, (ii) 130 nm deep × 1 μm wide grooves, (iii) 130 nm deep × 2 μm wide grooves and (iv) 130 nm deep × 4 μm wide grooves. Prior to use, grooved slides were soaked overnight in concentrated nitric acid, rinsed twice (30 min) with distilled water and sterilised with UV light. CECs align parallel to 130 nm deep nanogrooves (NGs) but groove width (1, 2 or 4 μm) did not affect alignment (Rajnicek et al., unpublished data) so in this study we pooled data for CECs migrating on 1, 2 or 4 μm widths.

### *Pharmacological reagents*

Drugs were dissolved directly in culture medium. Rho signalling was inhibited using 20 μg/ml C3 transferase isolated from *Clostridium botulinum* (BioMol Research Labs), which ADP-ribosylates rho (Vogelsgesang et al., 2007) and rho was activated using 1 μM L-α-lysophosphatidic acid (LPA) (Sigma) (Saito et al., 2004; Yamada et al., 2005; Pertz et al., 2006). A series of

selective, custom-made cell permeable peptides (Aberdeen University Proteomics Facility, Aberdeen, UK) were used to prevent signalling by rac, cdc42 or rho effector binding domains (10 μg/ml). The synthesis, specificity and efficacy of these compounds have been described (Vastrik et al., 1999; Dunican and Doherty, 2001; Rajnicek et al., 2006a). Cells were incubated in the peptides to allow uptake for at least 1 h prior to the start of the experiments. The rac and cdc42 inhibiting peptides correspond to amino acids 17–32 in their respective cdc42/rac1 binding (CRIB) domains. Rho inhibiting peptides corresponded to amino acids 23–40 of rho A (the class III binding domain) or 75–92 of rho A (the class I binding domain). All were tagged with the TAT internalisation sequence (GRKKRRQRRRPPQC) at the C terminus to facilitate membrane transport (Dunican and Doherty, 2001). We are confident that the TAT sequence does not affect peptide specificity since the rac and cdc42 peptides, which differ by only one amino acid and have identical TAT sequence tags, exert distinct behavioural and morphological effects (Rajnicek et al., 2006a and the present study). Effectors downstream of rho signalling were inhibited using peptides corresponding to the binding sites on rho A for citron kinase (amino acids 23–40) or rhotekin/rhophilin/protein kinase N (amino acids 75–92) (Fujisawa et al., 1998; Rajnicek et al., 2006a), and myosin light chain kinase and p160 rho kinase were inhibited by 2 mM butanedione monoxime (BDM) (Sigma) and 10 μM Y27632 (Tocris), respectively.

### *Electric field application*

Direct current electric fields (EFs) were applied using chambers prepared from 100 mm diameter plastic culture dishes (McCaig et al., 2005). Slides containing CECs were rinsed with medium 18 to 24 h after plating and were inverted (cell side down) over a drop of medium in the central trough of the 64 mm long × 10 mm wide × ~0.5 mm deep chamber. Medium was Minimal Essential Medium (MEM) with Hank's salts supplemented with 10% FBS, 25 mM HEPES, amino acid supplement, 2.5 μg/ml fungizone, 100 IU penicillin, 100 μg/ml streptomycin and 2 mM L-glutamine, pH 7.3 (all from Gibco-BRL). NGs were orthogonal to the EF unless stated otherwise. Electrical contact to the cells was from a direct current (DC) electrophoresis power supply connected to Ag/AgCl electrodes resting in saline-filled beakers, which in turn were connected to a drop of medium at each end of the slide by 20 cm long agar/salt bridges (McCaig et al., 2005). The EF strength was determined directly at the start of the experiment by measuring the voltage drop across the quartz slide and was monitored hourly.

### *Analysis of directed migration*

Visual fields incorporating the margins of the grooved regions were imaged (10× objective) at 0 h, 1 h and 3 h so cell movements could be monitored relative to fixed landmarks. Only cells migrating >2 μm/h and whose positions could be tracked reliably throughout the 3 h experiment were analysed since the spatial resolution was not sufficient to detect smaller cell movements. Data are presented as polar plots, in which the mean migration rate during the 3 h experiment is plotted against the angle of the migration vector for each cell relative to its initial position.

Directional cell migration after 3 h was quantified for each population by calculating a directional migration index as $\Sigma$ (cos $\theta$), where $\theta$ is the angle of each cell's net migration vector with 0° facing the cathode (or left), 180° facing the anode (or right), 90° facing up and 270° facing down (Fig. 1A). The index for a population would be +1 for migration directed perfectly towards the cathode, −1 directed towards the anode and 0 for migration directed vertically. A limitation of this analysis and others used previously to assess directed cell migration in EFs is that they cannot distinguish populations exhibiting random migration from those with perfectly balanced migration to the anode and cathode (or up and down), since each population would have an index of zero (Zhao et al., 1996b, 1999, 2006; McBain et al., 2003; Finkelstein et al., 2004; Pullar et al., 2001). It was essential that we distinguish these patterns since our experimental design (orthogonal presentation of NGs and EFs) was likely to produce orthogonally directed migration. Therefore, we also scored the frequency of cell migration into the quadrants facing the cathode (0±45°, or to left for no EF), the anode (180±45°, or to right for no EF), vertically up (90±45°) or down (270±45°). Initially cells migrating vertically up and those migrating vertically down were assessed as separate quadrants but no quantitative differences were identified under any experimental condition so they were combined subsequently to simplify presentation. Population frequencies were compared to those expected for random migration (25% left, 25% right; 50% up+down) and to those for cells on the same substrates exposed to an EF using a d-test (Bailey, 1981). Migration rates (mean±S.E.M.) were compared by an unpaired two-tailed Student's *t*-test.

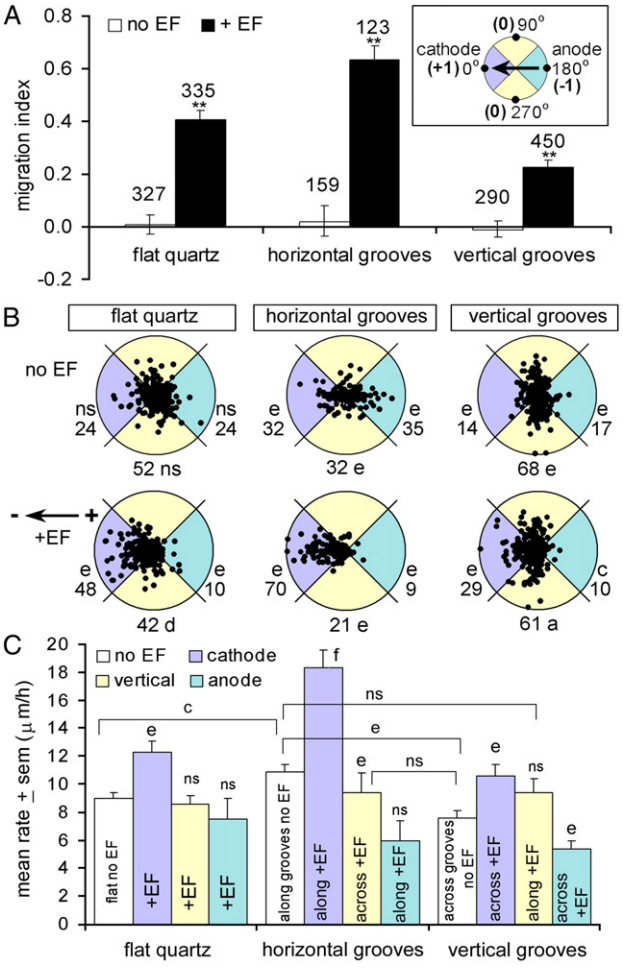


Fig. 1. Directional migration of bovine CECs on substratum 130 nm deep NGs and in an EF of 150 mV/mm. (A) The directional migration index describes the migration asymmetry in the horizontal axis and is calculated for each population as the mean (±S.E.M.) cos $\theta$, where $\theta$ is the angle of each cell's net migration path during 3 h as shown in the inset. The index is 0 for randomly directed migration (or for perfectly balanced migration restricted to the vertical or horizontal axis) and is −1 or +1 for migration directed exclusively towards the anode or cathode, respectively. The number of cells is indicated. $^{**}p<0.0001$ compared to no EF by two-tailed Student's *t*-test. (B) Plots of cell migration patterns for populations in panel A. Each cell started at the origin and its position after 3 h is shown. Radius 50 μm/h. The numbers beside the plots represent the % of cells in each segment (vertical segments are pooled). Letters indicate statistical significance for each segment by a D-test (Bailey, 1981). Frequencies for cells on flat quartz (no EF) were compared to the expected frequencies for randomly directed migration; 25% to the left (or cathode), 25% to the right (or anode) and 50% vertically (up+down) but cells exposed to an EF were compared to relevant control data (no EF). (a) $p<0.05$; (c) $p<0.01$; (e) $p<0.001$. (C) Directional migration rates for the cells in B. Letters above the coloured bars represent statistical comparisons to data for cells on the relevant substratum without an EF (white bar). Other comparisons are indicated by brackets. ns=not significant; (c) $p<0.01$; (e) $p<0.001$; (f) $p<0.0001$.

## Results

### *Corneal epithelial cells migrate parallel to nanogrooves (contact guidance)*

Bovine corneal epithelial cells migrated randomly on flat quartz in the absence of an EF, indicated by a directional migration index that approximates zero (Fig. 1A). The index for cells on grooved quartz (no EF) in which NGs were oriented horizontally or vertically also approximated zero, suggesting that NGs failed to direct CEC migration. However, this merely highlights a limitation of using the migration index in isolation to distinguish directed migration. Whilst truly random migration has a migration index of zero, when migration is restricted to the horizontal axis and is symmetrical (left/right) the migration index is also zero; as is symmetric migration along a vertical axis. Therefore, whilst the migration index is an efficient indicator of asymmetric left/right (or cathode/anode) migration in the horizontal axis, to identify selective migration along horizontal or vertical axes it is essential to use an additional analysis. Therefore, we used polar coordinate plots of the rate and direction of net migration to demonstrate the migration pattern for the population as well as to quantify the frequency of migration into quadrants facing directly towards the left (cathode), towards the right (anode) and the two vertical quadrants. This additional analysis confirmed that migration on flat quartz (no EF) was random (Fig. 1B) and that CECs migrated predominantly parallel to 130 nm deep NGs oriented along a horizontal or vertical axis. The migration index of approximately zero in each case (Fig. 1A) indicates that migration along the NG axis is symmetrical. CECs migrated faster parallel to NGs than on flat quartz and they migrated slower and less frequently across NGs (Fig. 1).

### *Corneal epithelial cells migrate towards the cathode of an EF on flat quartz (electrotaxis)*

Consistent with previous reports (Zhao et al., 1996b; McBain et al., 2003), the migration index and frequency of migration into the cathode-facing quadrant demonstrated that bovine CECs on a planar (flat) surface migrated preferentially towards the cathode of a 150 mV/mm EF (Fig. 1). Migration frequency into the anode-facing quadrant was significantly reduced. The EF also stimulated the rate of migration towards cathode relative to control cells (no EF) and relative to cells directed towards the anode (Fig. 1C).

### *Cathodal electrotaxis is enhanced when the EF and NGs are superimposed in parallel*

CECs in the eye migrate within arrays of parallel nano-scale fibrils whilst exposed simultaneously to an EF. Since CECs in vitro migrated parallel to NGs and preferentially towards the cathode of an EF when the stimuli were presented independently, we tested the possibility that directional migration could be improved by presenting NGs and an EF simultaneously, in parallel. Under those conditions the migration index indicated significant cathodal bias (Fig. 1A). Similarly, the frequency of migration along NGs into the cathodal quadrant was increased relative to cathodal migration on flat quartz or relative to migration towards the left (along NGs) in the absence of an EF (Fig. 1B). Polar plots demonstrated that when the EF and NGs were combined in parallel, migration was focused more directly towards the cathode than on flat quartz (Fig. 1B). Cells migrated about 50% faster towards the cathode along grooves than along NGs (no EF) or towards the cathode of EF (flat) in isolation (Fig. 1C). Therefore, when superimposed in parallel, an EF and substratum NGs increased the efficiency of cell migration directly towards the cathode substantially.

### *Establishing a hierarchy: contact guidance versus electrotaxis*

We explored the relative potencies of NGs and EFs in directing migration by exposing CECs migrating on NGs (130 nm deep) oriented vertically to an EF (150 mV/mm) oriented horizontally. This provided competing, orthogonal directional cues, effectively asking the cells to “choose” which cue was more potent. Four lines of evidence suggested that the EF dominated slightly: (1) The directional migration index was significantly larger than the near-zero value for CECs on vertical grooves without an EF (Fig. 1A), indicating a significant bias of migration across NGs towards the cathode. If vertical migration dominated, the index would be zero, as indicated by the data for control cells (no EF). (2) The frequency and rate of migration across grooves into the cathodal quadrant were greater than that across vertical NGs without an EF (Figs. 1B, C). (3) The frequency of migration parallel to NGs was reduced compared to that for CECs on vertical NGs in the absence of an EF (Fig. 1B). Therefore, the EF was sufficiently potent to recruit CECs from contact guidance to electrotaxis, overriding their normal tendency to avoid crossing NGs. (4) If vectoral electrotaxis and contact guidance contributed equally to the direction of cell movement, the migration vector for individual CECs would tend to lie at a 45° angle relative to the orthogonal cues. This is not apparent in polar plots (Fig. 1B). Instead, individual cells respond selectively, exhibiting either contact guidance or cathodal electrotaxis. Since the EF reduced the migration frequency along NGs, enhanced the migration rate and frequency towards the cathode, whilst also reducing the frequency and rate of anodal migration, we conclude that an EF of 150 mV/mm is a more potent directional cue than 130 nm deep NGs.

### *Electric field strength dependence*

All of the experiments described so far used an EF of 150 mV/mm. We tested CEC responses to smaller EFs (50 mV/mm) similar to those measured near corneal wounds in situ to explore the threshold for electrotaxis and we tested an EF at the higher end of the physiological range (250 mV/mm) in combination with orthogonal NGs (130 nm deep) to determine

whether the higher EF would override contact guidance completely. During 1 h of EF exposure, CECs on flat quartz migrated towards the cathode in an EF-strength-dependent manner (Fig. 2A). The migration index and migration rates for CECs on flat quartz demonstrated a significant cathodal bias at 150 or 250 mV/mm but not at 50 mV/mm. However, the frequency of migration into the cathode facing quadrant was significant even at 50 mV/mm (Figs. 2A, C, D). When NGs and the EF were co-presented orthogonally for 1 h, CECs migrated more frequently into the cathodal quadrant at EFs of 150 or 250 mV/mm, but not 50 mV/mm, but the migration index failed to show significant cathodal bias (Figs. 2A, C). After 3 h of EF exposure, the migration index for all EF strengths revealed significant cathodal bias on flat or NG substrata (Fig. 2B). In EFs of 250 mV/mm the migration index did not increase between 1 h and 3 h, however, suggesting that at EFs >50 mV/mm CECs achieve their maximum directional response within the first hour (Figs. 1A, B). Therefore, the threshold for cathodal CEC migration is at or below 50 mV/mm, but even 250 mV/mm failed to recruit the majority of cells from contact guidance to electrotaxis.

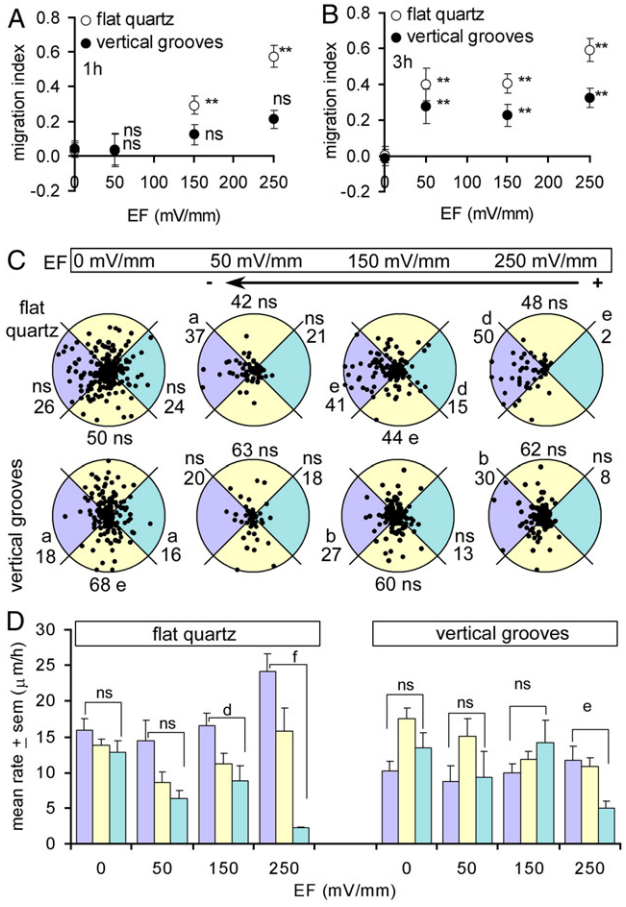


Fig. 2. EF strength-dependent cathodal migration. Cells were exposed to an EF for 1 h (A, C, D) or 3 h (B). Migration index calculations and polar plot formats and statistical comparisons are as in Fig. 1. The number of cells analysed ranged from 45 to 267 (A, C, D) and from 40 to 334 (B). Statistics are relative to no EF for cells on the relevant substratum; ns=not significant; $^{**}p<0.001$. (C) Polar plots for cells (1 h). Radius 50 μm/h. The numbers indicate the % of cells in each segment. ns=not significant; (a) $p<0.05$; (b) $p<0.02$; (d) $p<0.002$; (e) $p<0.001$. (D) Migration rates for the cells in C. Brackets compare cathodal and anodal rates by a two-tailed Student's *t*-test. ns=not significant; (d) $p<0.002$; (e) $p<0.001$; (f) $p<0.0001$.

*Rho GTPases mediate electrotaxis and contact guidance selectively*

The GTPases cdc42, rac and rho control spatial cytoskeletal dynamics and polarised cell migration. They have been implicated mechanistically in chemotaxis (Charest and Firtel, 2007) and electrotaxis (Rajnicek et al., 2006a,b) but their role in contact guidance by NGs is unknown. We explored the relative roles of cdc42 rac, and rho in contact guidance and electrotaxis separately, and in combination. Rho activity was either stimulated with LPA or attenuated with C3 transferase. Cdc42 and rac activities were disrupted using custom made peptides corresponding to the CRIB-binding domains (amino acids 17–32) of cdc42 or rac. These peptides have revealed selective roles for cdc42 and rac in cathodal electrotaxis of neuronal growth cones (Rajnicek et al., 2006a,b) and CEC alignment by EFs and NGs (data not shown).

The effects of rho GTPase modulation on electrotaxis (150 mV/mm for 3 h, flat quartz) are summarised in Fig. 3 and Table 1. Addition of peptide cdc42 17–32 to the culture medium abolished cathodal CEC electrotaxis. The migration index and cathodal migration frequency were indistinguishable from those for control cells (no EF). In addition to randomising, the direction of migration in the EF peptide cdc42 17–32 abolished the usual increase in migration rates for cells directed towards the cathode (Fig. 3C). Conversely, addition of peptide rac 17–32 to the medium did not affect electrotaxis. The migration index, the frequency of migration into each quadrant and the relatively rapid cathodal migration rates were similar to those for CECs in medium without any drug. Interestingly, CECs in medium containing C3 transferase (inactivates rho) exhibited greater cathodal electrotaxis as indicated by an increased migration index, increased frequency of migration into the cathode facing quadrant and increased migration rate for cells directed cathodally compared to those without the drug (Figs. 3A–C). Inclusion of LPA (activates rho) in the medium increased the directional migration index slightly (Fig. 3A), suggesting that rho elevation enhanced cathodal electrotaxis but analysis of the frequency of directional migration did not support this interpretation (Fig. 3B). Collectively, these data implicate signalling by cdc42 and rho but not rac in cathodal electrotaxis on planar surfaces.

Data for CEC contact guidance (130 nm deep NGs, no EF) are presented in the right side of Fig. 3 and are summarised in Table 1. The migration index values approximate zero, indicating that cells migrated predominantly along the vertical NG axis (Fig. 3A). This was confirmed by analysis of the frequencies of directional migration (Fig. 3B). Contact guidance along NGs was not affected by addition of peptides cdc42 17–32 or rac 17–32 to the medium but C3 transferase or LPA addition enhanced contact guidance (Supplemental Movies 1 and 2). Control (no drug, no EF) CECs migrated along NGs faster than across them and this relative increase

Table 1
Qualitative summary of directional responses for data in Figs. 3 and 4

| Treatment | Action | | EF alone [a] | NGs alone [b] | NGs+EF [c] |
|---|---|---|---|---|---|
| Cdc42 17–32 peptide | Attenuates Cdc42 signalling | Electrotaxis | ↓ | | ↓ |
| | | Contact guidance | | o | ↑ |
| Rac 17–32 peptide | Attenuates Rac signalling | Electrotaxis | o | | o |
| | | Contact guidance | | o | o |
| C3 transferase | Inactivates Rho signalling | Electrotaxis | ↑ | | ↑ |
| | | Contact guidance | | ↑ | o |
| LPA | Activates Rho signalling | Electrotaxis | o | | o |
| | | Contact guidance | | ↑ | ↑ |
| Rho 23–40 peptide | Attenuates Citron-K signalling | Electrotaxis | ↑ | | ↑ |
| | | Contact guidance | | o | ↓ |
| Rho 75–92 peptide | Attenuates rhotekin signalling | Electrotaxis | o | | o |
| | | Contact guidance | | ↑ | o |
| Y27632 | Attenuates ROCK signalling | Electrotaxis | o | | o |
| | | Contact guidance | | ↑ | ↑ |
| BDM | Attenuates MLCK signalling | Electrotaxis | o | | o |
| | | Contact guidance | | ↑ | o |

↓=reduced directed migration; ↑=increased directed migration; o=no effect on directed migration.
[a] CECs on flat quartz+EF compared to CECs on flat quartz+EF without any drug in the medium.
[b] CECs on NGs without an EF. Responses are compared to CECs on NGs without an EF or drug.
[c] CECs on NGs+EF. Responses are compared to CECs on NGs+EF without any drug in the medium.

was sustained in medium containing C3 transferase or LPA but not cdc42 17–32, or rac 17–32 (yellow bars compared to green or blue bars in Fig. 3C). Therefore, directional contact guidance involves signalling via rho but not via rac or cdc42 in isolation.

When the EF (150 mV/mm) and 130 nm deep grooves were co-presented orthogonally for 3 h, the inhibitors produced a range of effects on migration patterns (extreme right of Fig. 3, Table 1). Consistent with electrotaxis data for CECs on flat quartz, peptide cdc42 17–32 reduced the migration index and reduced the frequency of cell migration across grooves into the cathode-facing quadrant. Interestingly, peptide cdc42 17–32 enhanced the rate and frequency of migration along grooves compared to controls (no drug, vertical NGs, EF). Therefore, attenuating cdc42 activity favoured contact guidance over electrotaxis. Consistent with the EF response on flat quartz and the contact guidance response in the absence of an EF, peptide rac 17–32 did not affect the migration index or the frequency of migration towards the cathode or along NGs. However, C3 transferase enhanced the migration index and the frequency of migration across NGs towards the cathode, mimicking its enhancement of cathodal electrotaxis on flat quartz, and decreased the frequency of migration towards the anode, but C3 transferase did not increase the migration frequency along NGs, as it had in the absence of an EF. In some cases, CECs migrated along NGs for the first hour in the EF and then migrated directly towards the cathode for the subsequent 2 h, even as sheets of cells (Supplemental Movie 3), suggesting a temporal mechanistic switch from contact guidance to electrotaxis. LPA did not affect the migration index or the frequency of cathodal migration across NGs compared to no drug controls but it enhanced the migration frequency along NGs. Therefore, attenuation of rho signalling prioritised electrotaxis over contact guidance and activation of rho prioritised contact guidance over electrotaxis.

### *Rho GTPase effectors*

Having implicated rho signalling in both electrotaxis and contact guidance, we tested the hypothesis that directed migration involved the rho effectors myosin light chain kinase (MLCK), p160 rho-associated coil-containing protein kinase (ROCK), citron kinase (citron-K) or rhophilin/rhotekin/protein kinase N (PKN). These molecules modulate cytoskeleton dynamics and have been implicated in cathodal electrotaxis of neuronal growth cones (Rajnicek et al., 2006a). Citron-K activity was inhibited by a custom made peptide corresponding to amino acid residues 23–40 on rhoA (rho 23–40) and rhophilin/rhotekin/PKN activity was inhibited by a peptide corresponding to residues 75–92 on rhoA (rho 75–92).

The directional migration data in Fig. 4 are summarised in Table 1. The rho 23–40 peptide increased the migration index for cells on flat or NG substrata compared to that without the peptide. Analysis of directional migration frequencies revealed that increased electrotaxis towards the cathode (across NGs) was at the expense of contact guidance but the peptide did not affect contact guidance in the absence of an EF (Fig. 4B). Conversely, rho 75–92 enhanced contact guidance in the absence of an EF but had no effect on cathodal electrotaxis on flat or NG quartz (Figs. 4A, B). The ROCK inhibitor Y27632 and BDM, which inhibits MLCK activity, each enhanced contact guidance in the absence of an EF and did not affect cathodal electrotaxis on flat quartz. When grooves and an EF were co-presented, however, the directional responses for cells in medium containing Y27632 mimicked those for cells presented with each cue independently (enhanced contact guidance, no effect on electrotaxis). BDM did not affect directional electrotaxis or contact guidance (Fig. 4).

All inhibitors prevented the usual increase in migration rate for cells directed along NGs in the absence of an EF (Fig. 4C). Peptide rho 23–40 and Y27632 also eliminated the

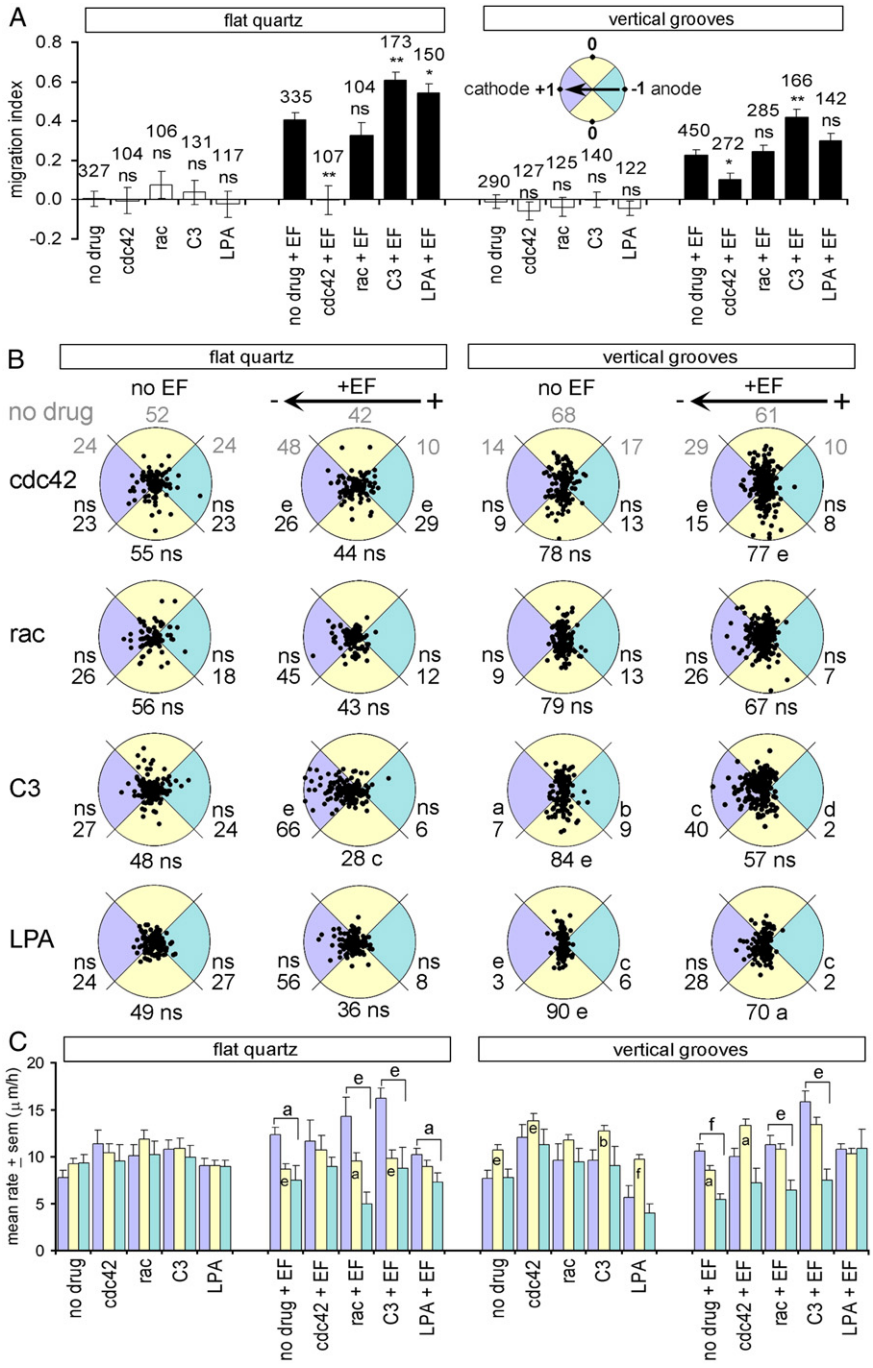


Fig. 3. The influence of signalling by cdc42, rac and rho on directional migration. NGs are 130 nm deep and the EF is 150 mV/mm (3 h). (A) The migration index describes asymmetry of migration in the horizontal axis and is calculated as shown in the inset and in Fig. 1A. Number of cells is shown above each bar. Statistics are relative to no drug controls (first bar in each series); ns = no significant difference; *$p<0.05$, **$p<0.0001$ compared to no EF by two-tailed Student's *t*-test. (B) Polar plots of migration for the cells in panel A. Radius is 50 μm/h. Numbers indicate the frequency of migration into each segment (% total). Control values (grey text, no EF) are repeated from Fig. 1B for ease of comparison. Letters indicate statistical significance relative to no drug controls; except for frequencies on flat quartz without an EF, which are compared to the expected frequencies for randomly directed migration (D-test; Bailey, 1981). (a) $p<0.05$; (b) $p<0.02$; (c) $p<0.01$; (d) $p<0.002$; (e) $p<0.001$. (C) Directional migration rates for cells in panel B. Statistics (two-tailed Student's *t*-test) for cells migrating vertically on flat quartz in an EF (letters in yellow bars) are relative to cells migrating vertically (yellow) on flat quartz (no drug). Cells migrating vertically on NGs (yellow bars) are compared to relevant no drug control cells migrating vertically. Brackets compare relative rates of cathodal and anodal migration. Where no *p* value is indicated the rates are not significantly different. (a) $p<0.05$; (b) $p<0.02$; (c) $p<0,01$; (d) $p<0.002$; (e) $p<0.001$; (f) $p<0.0001$.

EF-stimulated enhancement of cathodal migration rates compared to anodal rates on flat quartz, although this was retained for EF-treated cells on NGs in the presence of peptide rho 23–40.

## Discussion

During development, embryonic cells often migrate to distant destinations. On route they encounter multiple gradients

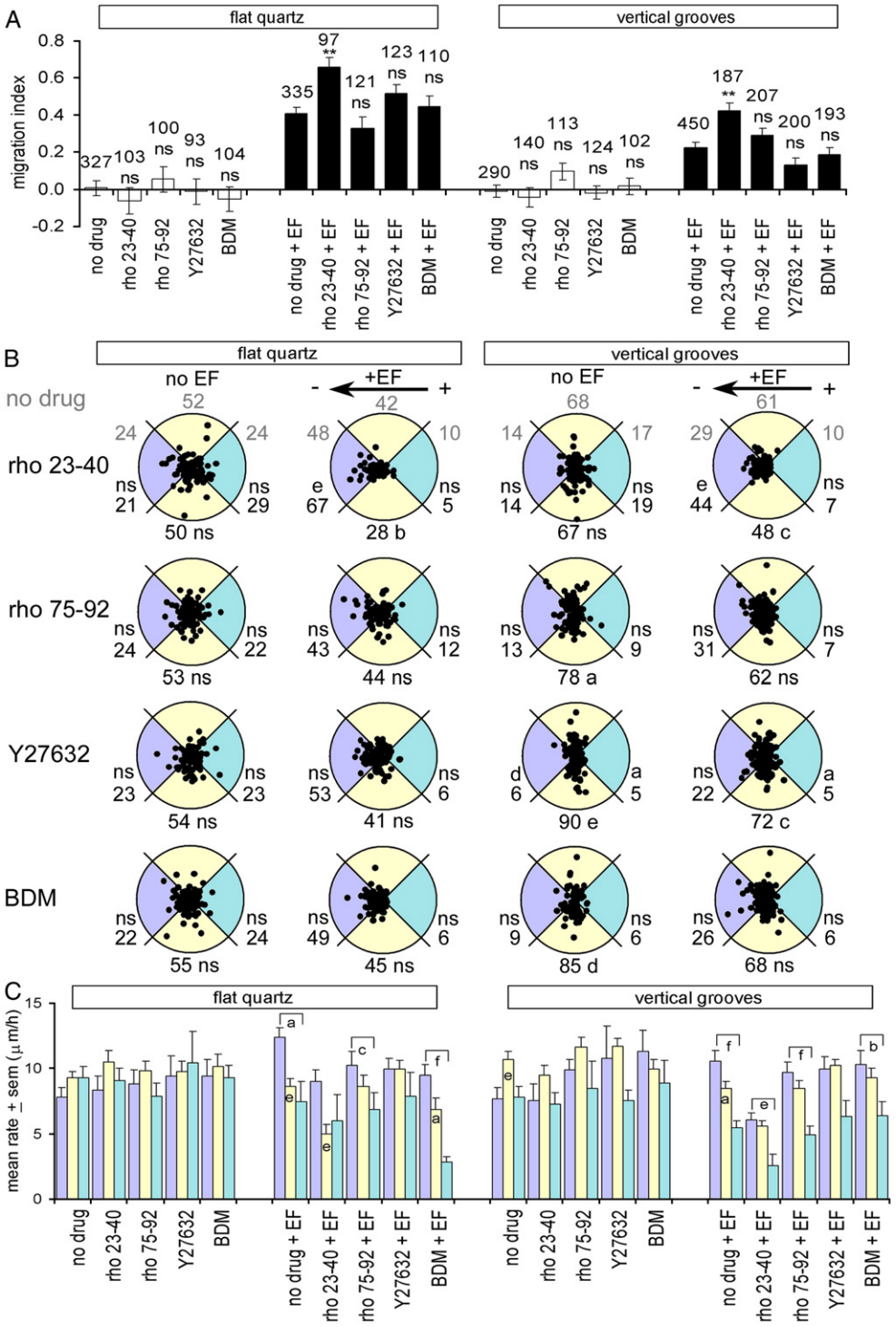


Fig. 4. The influence of rho effectors on directional migration. Format for presentation and statistical comparisons as in Fig. 3. (A) The migration index is calculated as in Fig. 1A. NGs are 130 nm deep; EF is 150 mV/mm (3 h). Statistics compare the migration index for populations in inhibitor-containing medium to those without any drug. ns = no significant difference, $^{**}p < 0.001$ by a two-tailed Student's *t*-test. (B) Polar plots of migration for the cells in panel A. Radius is 50 μm/h. The numbers represent the % cells in each segment. Control (no drug) frequencies are repeated from Fig. 1B. ns = no significant difference; (a) $p < 0.05$; (b) $p < 0.02$; (c) $p < 0{,}01$; (e) $p < 0.001$. (C) Directional migration rates for cells in panel B.

and tracks of extracellular molecules, whilst simultaneously navigating three-dimensional spaces. A similar process operates during wound healing, where vectoral cues within the wound milieu direct epithelial cell migration towards the injury. Considered in isolation, each of the many, co-existing extracellular signals has the potential to facilitate (or impede) directional cell migration. How cells sense overlapping, potentially contradictory, cues and the intracellular mechanisms by which they translate them into coordinated movement is a fundamental unresolved question. We addressed this issue directly with a

novel in vitro assay that permits precise spatial control of overlapping vectoral cues. Our data implicate the signalling molecules rho and cdc42 in polarized CEC migration by substratum topography and by a steady DC electric field, cues that co-exist in the wounded cornea. The data are central to the principles of direction sensing by cells.

### *CECs migrate preferentially along substratum grooves (contact guidance)*

Transparency of the cornea is the consequence of a remarkable microanatomy, in which parallel collagen fibrils 20–40 nm in diameter are organised into densely packed, orthogonally interwoven lamellae 7 μm to 250 μm wide and 200 nm to 2 μm deep (Holmes et al., 2001; Komai and Ushiki, 1991; Ojeda et al., 2001). Cells of the overlying epithelium may migrate directly over the denuded stroma to reepithelialise a wound (Suzuki et al., 2003) so if substratum topography guides CEC migration, the orientated collagen lamellae could affect healing. Therefore, understanding how CECs sense subtle topographic anisotropy and translate it into polarised migration is relevant clinically.

Our observations that bovine CECs migrated more frequently and faster parallel to 130 nm deep substratum nanogrooves (NGs) than across NGs or on flat (ungrooved) quartz in the absence of an EF are consistent with reports for migration of individual CECs on deeper (400 nm to 5 μm) grooves (Dalton et al., 2001; Diehl et al., 2005) but contrast with those for human CECs on 150 or 600 nm deep NGs (70 nm to 2.1 μm widths), which migrate randomly and more slowly on grooved than planar surfaces (Teixeira et al., 2003). Artificial NGs as shallow as 130 nm have not been reported to direct cell migration (Flemming et al., 1999).

### *CEC migration along nanogrooves is mediated by rho*

Spatially and temporally coordinated activities of the small GTPases rac, cdc42 and rho are proposed to underpin polarised cell migration of a variety of cells, including CECs (Charest and Firtel, 2007; Raftopoulou and Hall, 2004; Nakamura et al., 2001; Hall, 2005; Kimura et al., 2006). This idea, developed initially for chemotaxis, has been extended recently to electrotaxis, with the cathode as the attractant (Rajnicek et al., 2006a,b). By this model activities of rac and cdc42 are elevated on the side of the cell facing the attractant but rho activity is low. Conversely, on the side of the cell facing away from the attractant, rho activity is high, with relatively low cdc42 and rac activities. The transcellular gradient is reinforced by mutual antagonism of rac/cdc42 and rho. Migration towards the attractive stimulus arises from protrusion of filopodia and a lamellipodium at the leading edge via cdc42 and rac signals, and retraction of the trailing edge via rho-mediated actomyosin contraction.

The mechanism for directed migration along NGs (contact guidance) remains unknown but leading edge CEC filopodia and lamellipodia are influenced by substratum contours (Teixeira et al., 2006; Dalton et al., 2001; Karuri et al., 2004). Therefore we tested the requirements for rac and cdc42 in contact guidance using peptides that prevent signalling by rac or cdc42 effectors (Rajnicek et al., 2006a,b; Vastrik et al., 1999). Sustained contact guidance of CECs (no EF) in medium containing the rac peptide is consistent with sustained chemotropism of rac null macrophages (Wheeler et al., 2006). In motile cells cdc42 and rac are proposed to act co-ordinately to control directional sensing and migration, respectively (Charest and Firtel, 2007; Hall 2005) so we were surprised that cdc42 attenuation also failed to affect contact guidance. This suggests that other signals compensate for attenuated cdc42 or rac activity. Alternatively, the canonical roles for rac and cdc42 derived for chemotropism on planar substrata may not apply to contact guidance on NGs, perhaps the result of altered gene expression on nano-textured substrata (Dalby et al., 2002).

Efficient contact guidance comprises steering and speed. Treatment of CECs with the cdc42 or rac peptides did not affect steering but did prevent the inherent increase of migration speed along NGs compared to that across NGs. Therefore, interplay between rac and cdc42 signals may be necessary to optimise contact guidance efficiency. We discounted the possibility that the peptides failed to affect rac or cdc42 signalling because they influenced cell morphology (data not shown), alignment on NGs (data not shown) and electrotaxis (Fig. 3) distinctly.

Rho signalling was pivotal for CEC contact guidance (no EF). Drugs that attenuated (C3 transferase) or stimulated (LPA) rho activity in CECs (Nakamura et al., 2001; Saito et al., 2004) enhanced the frequency of migration along NGs. By attenuating effectors downstream of rho, we implicated ROCK, MLCK and PKN-related signalling (our peptide does not distinguish between rhophilin, rhotekin and PKN) mechanistically but not citron kinase. We propose that the physical discontinuities of parallel substratum NGs alter the balance of rho activity locally by an unidentified mechanism that encourages cell to substratum adhesions preferentially on ridges. Anisotropic cytoskeletal contraction then generates a bipolar, aligned morphology with lamellipodia extension at either apex. One arbitrarily becomes the nascent leading edge, moving along the NGs, perhaps via “frontal towing” (Petroll et al., 2003) with new adhesions forming at ridge contacts. Several observations support this proposal: (1) CECs on NGs are “fried egg” shaped soon after plating with cortical actin stripes coincident with substratum ridges. Subsequently, lamellipodia protrude (or are retained selectively) at ridges and the cell elongates, acquiring a bipolar morphology (data not shown). Similar events underlie macrophage alignment to NGs as shallow as 30 nm (Wojciak-Stothard et al., 1996). (2) Ridge-associated stripes of actin persist within lamellipodia and the cell body of CECs on NGs (data not shown; Teixeira et al., 2006). (3) Focal contacts localise with and align to substratum ridges, thus polarising the cell’s contractile and traction-generating machinery relative to NGs (den Braber et al., 1998; Dalton et al., 2001; Teixeira et al., 2006). (4) CEC contact guidance is affected by manipulation of rho and its effectors, including ROCK which is present in CECs (Nakamura et al., 2001) and mediates cytoskeletal contraction.

(5) Corneal fibroblasts on fibrillar collagen matrices are bipolar. Their polarised alignment and migration in response to substratum-induced strain are controlled by ROCK-dependent substratum adhesions in the leading lamellipodium (Petroll et al., 2003, 2004a,b).

Migration of rabbit corneal epithelial sheets was stimulated by LPA and was attenuated by C3 transferase in organ culture (Nakamura et al., 2001) so it is not clear why LPA and C3 transferase enhanced bovine CEC contact guidance in our experiments. It might reflect mechanistic differences between migration of cell sheets and isolated cells or it may indicate that any shift in rho equilibrium enhances the subtle, localised changes in rho activity proposed to underpin contact guidance of isolated CECs.

*CECs migrate towards the cathode (electrotaxis)*

Consistent with previous studies, CECs on planar substrata migrated towards the cathode of an EF (Soong et al., 1990; Zhao et al., 1996a,b, 2006, Farboud et al., 2000). This is important because CECs reepithelialise wounds within the context of a naturally-occurring EF. The EF is a consequence of polarised ion transport across the intact epithelium, which establishes an inwardly positive transepithelial potential (TEP) of 40 mV (Song et al., 2004; McCaig et al., 2005), thus acting as an "epithelial battery". Upon wounding the TEP collapses instantly to 0 mV at the wound, but is maintained as normal distally (~1 mm away). The resulting TEP gradient establishes an EF within the tissues adjacent to (parallel to) the epithelium with the wound as the cathode. In mammalian epithelium, EFs ranging from 40 to 200 mV/mm have been measured near the wound edge (Barker et al., 1982; Chiang et al., 1992; Sta Iglesia and Vanable, 1998). A wound-induced EF of 42 mV/mm has been measured in the bovine cornea (Chiang et al., 1992; but probably underestimated) but most previous studies of CEC electrotaxis in vitro have used EFs of 100 mV/mm or higher. Here we show cathodal electrotaxis of isolated CECs on flat quartz in EFs spanning the entire physiological range (50 to 250 mV/mm). Collectively, our data for electrotaxis of single cells at 50 mV/mm, together with data from an in situ bovine eye preparation (EF 80 mV/mm; Sta Iglesia and Vanable, 1998) and a bovine CEC monolayer wound model (EF of 50 mV/mm; Zhao et al., 2006) support the assertion that electrotaxis contributes to corneal reepithelialisation in situ.

*Electrotaxis on planar quartz involves signalling by cdc42 and rho but not rac*

Some mechanistic components for CEC cathodal electrotaxis have been identified, including asymmetric distribution (or activation) of membrane receptors for growth factors and activity of phosphate and tensin homolog deleted on chromosome ten (PTEN) and phosphoinositide kinase (PI3K) (Zhao et al., 1996b, 2006; McBain et al., 2003; McCaig et al., 2005; Pullar et al., 2007). Of all inhibitors tested here only the cdc42 inhibiting peptide abolished electrotaxis completely on flat quartz, indicating that cdc42 activity is pivotal. Cdc42 activation excludes PTEN from the leading edge of migrating cells (Charest and Firtel, 2007) so in Fig. 5 we propose a model by which crosstalk between cdc42 and PTEN mediates electrotaxis. Rho, which is segregated spatially to the rear of migrating cells and is elevated on the anode-facing sides of neuronal growth cones (Rajnicek et al., 2006a) activates PTEN via ROCK (Charest and Firtel, 2007). Cathodal electrotaxis is enhanced in PTEN null mutant keratinocytes (Zhao et al., 2006) as were our CECs upon attenuation of rho activity. However, our data implicate citron-K, not ROCK, as the rho effector since Y27632 failed to affect electrotaxis but citron-K attenuation (with peptide rho 23–40) enhanced electrotaxis similarly to rho attenuation (with C3 transferase). Interestingly, inhibitors of rho effectors revealed complementary effects on electrotaxis and contact guidance (Table 1), suggesting that effectors downstream of rho may activate divergent signals to prioritise co-existing directional cues. We did not identify a role for rac in polarised CEC migration, but in neuronal growth cones the same rac peptide abolished cathodal steering (Rajnicek et al.,

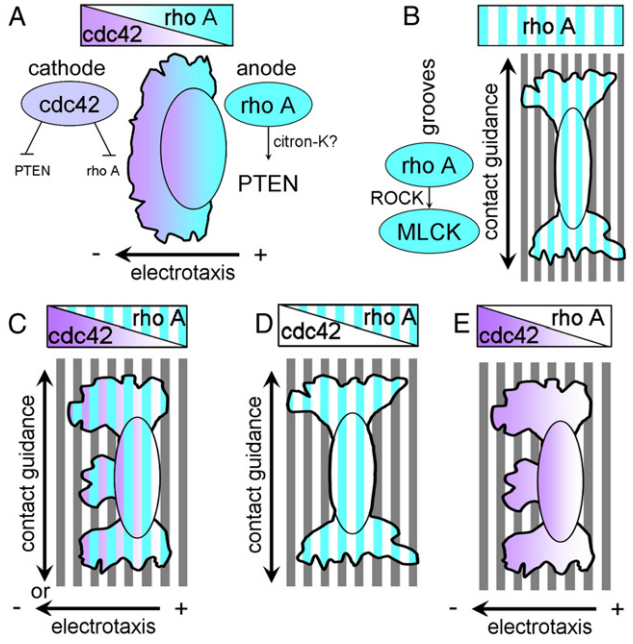


Fig. 5. Hypothetical mechanism underpinning electrotaxis and contact guidance. (A) Cell on a planar substratum exposed to an EF. Cdc42 signalling dominates in the cathode facing plasma membrane (purple) and activities of PTEN and rho are relatively low. Conversely, on the anode-facing membrane rho activity is relatively high (blue), which stimulates PTEN activity. Our data suggest that citron-K acts downstream of rho in electrotaxis. (B) Cell on vertical NGs (white stripes) in the absence of an EF (no drug added). Rho is activated selectively on ridges (blue stripes). This may stimulate contact guidance (double headed arrow) by localised activation of rho-kinase (ROCK) and myosin light chain kinase (MLCK), which polarise traction and force generating activities. Our data support roles for ROCK and MLCK in contact guidance. (C–E) Superimposition of an EF and vertical NGs. (C) In normal medium, cells migrate either towards the cathode or along NGs. Interplay between cdc42 and rho signalling determines the dominant guidance cue because contact guidance is enhanced when cdc42 is attenuated (D) and when rho activity is attenuated cells are converted from contact guidance to electrotaxis (E).

2006a,b), thus revealing differences in electrotaxis mechanisms in different cell types.

*Establishing a hierarchy: contact guidance versus electrotaxis*

Cells migrating in vivo are confronted with an astounding variety of potential vectoral cues. The question of how cells interpret them is fundamental to embryonic development, wound healing and tumour metastasis. Unfortunately, the complexities of experimental design and data interpretation have restricted attempts to study responses of cells to superimposed vectoral cues (Bromberek et al., 2002; Britland and McCaig, 1996; Britland et al., 1996). We have studied the interplay of spatially controlled physical (NGs) and electrical cues by superimposing NGs and an EF in parallel (co-operative cues) to reveal that the frequency and rate of migration towards the cathode were improved compared to either cue in isolation. Although not surprising, this was satisfying since it verifies the potential for combinations of these cues to be exploited in bioengineering or novel wound healing therapies.

We also superimposed the cues orthogonally (vertical NGs, horizontal EF) to establish a hierarchy for contact guidance versus electrotaxis. Interestingly, cells "chose" one or the other cue; some migrated vertically along NGs and others migrated directly across NGs towards the cathode. If the cues were equally potent, the vectoral sum of electrotaxis (0°) and contact guidance (90°) would be integrated to yield a net migration vector of ~45° but this was not apparent in our data. Although some cells migrated initially via contact guidance then switched to electrotaxis (Supplemental Movie 3), responses were selective, not integrative.

We conclude that a mechanistic "cdc42/rho switch" determines the dominant cue because (flat quartz) cdc42 attenuation abolishes cathodal electrotaxis and rho attenuation enhances electrotaxis and on NGs (no EF) modulating rho activity enhances contact guidance. Baseline rho activity is pivotal in the directional choice because when NGs and an EF were presented orthogonally attenuation of rho signalling favoured electrotaxis and rho stimulation favoured contact guidance. A mechanistic model is presented in Fig. 5.

Our data indicate that the EF (150 mV/mm) is a more potent stimulus than contact guidance by NGs (130 nm deep) because when NGs and an EF were oriented orthogonally CEC migration along NGs was reduced and cathodal electrotaxis was increased. Therefore, electrotaxis occurred at the expense of contact guidance. The EF was a sufficiently potent stimulus for CECs to overcome their normal aversion to crossing NGs to migrate directly towards the cathode. However, even increasing the EF to 250 mV/mm was not sufficient to convert the majority of cells to electrotaxis, suggesting that although the EF is more potent it is not a dominant cue. It has been hypothesised that a gradient of soluble chemoattractants controls wound healing but cathodal electrotaxis persisted in monolayer wounds with continuous perfusion of medium, suggesting that electrical cues override coincident chemotropic cues (Zhao et al., 2006). Our data suggest a similar hierarchy, prioritising electrotaxis over subtle topography.

Our data are relevant to normal corneal maintenance. The corneal limbus (the corneal/scleral boundary) has a circumferential collagen fibril organisation distinct from that in the central cornea and contains a stem cell population from which CECs migrate centripetally to replace those sloughed naturally from the central cornea. The migration path from the limbus has a striking spiral shape but its basis is not known (Collinson et al., 2004). Our data suggest that the curved pattern may arise from regional variation in corneal microanatomy, perhaps in combination with the natural EF.

## Acknowledgments

W. Monaghan, C. Wilkinson and A. Curtis at The University of Glasgow prepared the grooved substrata.

## Appendix A. Supplementary data

Supplementary data associated with this article can be found, in the online version, at doi:10.1016/j.ydbio.2007.09.051.

## References

Bailey, N.T.J., 1981. Statistical Methods in Biology, 2nd edn. Hodder and Stoughton, London, pp. 38–39.

Barker, A.T., Jaffe, L.F., Vanable, J.W., 1982. The glabrous epidermis of cavies contains a powerful battery. Am. J. Physiol.: Regul. Integr. Comp. Physiol. 242, R358–R366.

Britland, S., McCaig, C., 1996. Embryonic *Xenopus* neurites integrate and respond to simultaneous electrical and adhesive guidance cues. Exp. Cell Res. 225, 31–38.

Britland, S., Morgan, H., Wojiak-Stodart, B., Riehle, M., Curtis, A., Wilkinson, C., 1996. Synergistic and hierarchical adhesive and topographic guidance of BHK cells. Exp. Cell Res. 228, 313–325.

Bromberek, B.A., Enver, P.A.J., Shreiber, D.I., Caldwell, M.D., Tranquillo, R.T., 2002. Macrophages influence a competition of contact guidance and chemotaxis for fibroblast alignment in a fibrin gel coculture assay. Exp. Cell Res. 275, 230–242.

Charest, P.G., Firtel, R.A., 2007. Big roles for small GTPases in the control of directed cell movement. Biochem. J. 401, 377–390.

Chiang, M., Robinson, K.R., Vanable, J.W., 1992. Electrical fields in the vicinity of epithelial wounds in the isolated bovine eye. Exp. Eye Res. 54, 999–1003.

Collinson, J.M., Chanas, S.A., Hill, R.E., West, J.D., 2004. Corneal development, limbal stem cell function, and corneal epithelial cell migration in the Pax6−/− mouse. Investig. Ophthalmol. Vis. Sci. 45, 1101–1108.

Dalby, M.J., Yarwood, S.J., Riehle, M.O., Johnstone, H.J.H., Affrossman, S., Curtis, A.S.G., 2002. Increasing fibroblast response to materials using nanotopography: morphological and genetic measurement of cell response to 13 nm-high polymer demixed islands. Exp. Cell Res. 276, 1–9.

Dalton, B.A., Walboomers, X.F., Dziegielewski, M., Evans, D.M., Taylor, S., Jansen, J.A., Steele, J.G., 2001. Modulation of epithelial tissue and cell migration by microgrooves. J. Biomed. Mater. Res. 56, 195–207.

den Braber, E.T., de Ruijter, J.E., Ginsel, L.A., von Recum, A.F., Jansen, J.A., 1998. Orientation of ECM protein deposition, fibroblast cytoskeleton, and attachment complex components on silicone microgrooved surfaces. J. Biomed. Mater. Res. 40, 291–300.

Diehl, K.A., Foley, J.D., Nealey, P.F., Murphy, D.J., 2005. Nanoscale topography modulates corneal epithelial cell migration. J. Biomed. Mater. Res. 75A, 603–611.

Dunican, D.J., Doherty, P., 2001. Designing cell permeant phosphopeptides to modulate intracellular signalling pathways. Biopolymers 60, 45–60.

Evans, M.D.M., McFarland, G.A., Taylor, S., Walboomers, X.F., 2005. The response of healing corneal epithelium to grooved polymer surfaces. Biomaterials 26, 1703–1711.

Farboud, B., Nuccitelli, R., Schwab, I.R., Isseroff, R.R., 2000. DC electric fields induce rapid directional migration in cultured human corneal epithelial cells. Exp. Eye Res. 70, 667–673.

Finkelstein, E., Chang, W., Chao, P.H.G., Gruber, D., Minden, A., Hung, C.T., Bulinski, J.C., 2004. Roles of microtubules, cell polarity and adhesion in electric-field-mediated motility of 3T3 fibroblasts. J. Cell. Sci. 117, 1533–1545.

Flemming, R.G., Murphy, C.J., Abrams, G.A., Goodman, S.L., Nealey, P.F., 1999. Effects of synthetic micro- and nano-structured surfaces on cell behaviour. Biomaterials 20, 573–588.

Fujisawa, K., Madaule, P., Ishizaki, T., Watanabe, G., Bito, H., Saito, Y., Hall, A., Narumia, S., 1998. Different regions of Rho determine Rho-selective binding of different classes of Rho target molecules. J. Biol. Chem. 273, 18943–18949.

Gipson, I.K., Grill, S.M., 1982. A technique for obtaining sheets of intact rabbit corneal epithelium. Investig. Ophthal. Vis. Sci. 23, 269–273.

Hall, A., 2005. Rho GTPases and the control of cell behaviour. Biochem. Soc. Trans. 33, 891–895.

Holmes, D.F., Gilpin, C.J., Baldock, C., Ziese, U., Koster, A.J., Kadler, K.E., 2001. Corneal collagen fibril structure in three dimensions: structural insights into fibril assembly, mechanical properties, and tissue organization. Proc. Natl. Acad. Sci. 98, 7307–7312.

Karuri, N.W., Liliensiek, S., Teixeira, A.I., Abrams, G., Campbell, S., Nealey, P.F., Murphy, C.J., 2004. Biological length scale topography enhances cell-substratum adhesion of human corneal epithelial cells. J. Cell. Sci. 117, 3153–3164.

Kimura, K., Kawamoto, K., Teranishi, S., Nishida, T., 2006. Role of rac1 in fibronectin-induced adhesion and motility of human corneal epithelial cells. Investig. Ophthalmol. Vis. Sci. 47, 4323–4329.

Komai, Y., Ushiki, T., 1991. The three-dimensional organization of collagen fibrils in the human cornea and sclera. Investig. Ophthalmol. Vis. Sci. 32, 2244–2258.

Maurice, D.M., 1957. The structure and transparency of the cornea. J. Physiol. 136, 263–286.

McBain, V.A., Forrester, J.V., McCaig, C.D., 2003. HGF, MAPK, and a small physiological electric field interact during corneal epithelial cell migration. Investig. Ophthalmol. Vis. Sci. 44, 540–547.

McCaig, C.D., Rajnicek, C.D., Song, B., Zhao, M., 2005. Controlling cell behaviour electrically: current views and future potential. Physiol. Rev. 85, 943–978.

Nakamura, M., Nagano, T., Chikama, T., Nishida, T., 2001. Role of the small GTP-binding protein rho in epithelial cell migration in the rabbit cornea. Investig. Ophthalmol. Vis. Sci. 42, 941–947.

Ojeda, J.L., Ventosa, J.A., Piedra, S., 2001. The three-dimensional micro-anatomy of the rabbit and human cornea. A chemical and mechanical microdissection-SEM approach. J. Anat. 199, 567–576.

Pertz, O., Hodgson, L., Klemke, R.L., Hahn, K.M., 2006. Spatiotemporal dynamics of rho A activity in migrating cells. Nature 440, 1069–1072.

Petroll, W.M., Ma, L., Jester, J.V., 2003. Direct correlation of collagen matrix deformation with focal adhesion dynamics in living corneal fibroblasts. J. Cell. Sci. 116, 1481–1491.

Petroll, W.M., Cavanagh, H.D., Jester, J.V., 2004a. Dynamic three-dimensional visualisation of collagen matrix remodelling and cytoskeletal organization in living corneal fibroblasts. Scanning 26, 1–10.

Petroll, M.W., Vishwanath, M., Ma, L., 2004b. Corneal fibroblasts respond rapidly to changes in local mechanical stress. Investig. Ophthalmol. Vis. Sci. 45, 3466–3474.

Pullar, C.E., Isseroff, R.R., Nuccitelli, R., 2001. Cyclic AMP-dependent protein kinase A plays a role in the directed migration of human keratinocytes in a DC electric field. Cell Motil. Cytoskelet. 50, 207–217.

Pullar, C.E., Zhao, M., Song, B., Pu, J., Reid, B., Ghoghawala, S., McCaig, C., Isseroff, R.R., 2007. Beta-adrenergic receptor agonists delay while antagonists accelerate epithelial wound healing: evidence of an endogenous adrenergic network within the corneal epithelium. J. Cell. Physiol. 211, 261–272.

Raftopoulou, M., Hall, A., 2004. Cell migration: rho GTPases lead the way. Dev. Biol. 265, 23–32.

Rajnicek, A.M., Britland, S., McCaig, C.D., 1997. Contact guidance of CNS neurites on grooved quartz: influence of groove dimensions, neuronal age and cell type. J. Cell. Sci. 110, 2905–2913.

Rajnicek, A.M., Foubister, L.E., McCaig, C.D., 2006a. Temporally and spatially coordinated roles for rho, rac, cdc42 and their effectors in growth cone guidance by a physiological electric field. J. Cell. Sci. 119, 1723–1735.

Rajnicek, A.M., Foubister, L.E., McCaig, C.D., 2006b. Growth cone steering by a physiological electric field requires dynamic microtubules, microfilaments and rac-mediated filopodial asymmetry. J. Cell. Sci. 119, 1736–1745.

Reid, B., Song, B., McCaig, C.D., Zhao, M., 2005. Wound healing in rat cornea: the role of electric currents. FASEB J. 19, 379–386.

Saito, J., Morishige, N., Chikama, T., Gu, J., Sekiguchi, K., Mishida, T., 2004. Differential regulation of focal adhesion kinase and paxillin phosphorylation by the small GTP-binding protein rho in human corneal epithelial cells. Jpn. J. Ophthalmol. 48, 199–207.

Song, B., Zhao, M., Forrester, J.V., McCaig, C.D., 2004. Nerves are guided and nerve sprouting is stimulated by a naturally occurring electrical field in vivo. J. Cell. Sci. 117, 4681–4690.

Soong, H.K., Parkinson, W.C., Bafna, S., Sulik, G.L., Huang, S.C., 1990. Movements of cultured corneal epithelial cells and stromal fibroblasts in electric fields. Investig. Ophthalmol. Vis. Sci. 31, 2278–2282.

Sta Iglesia, D.D., Vanable, J.W., 1998. Endogenous lateral electric fields around bovine corneal lesions are necessary for and can enhance normal rates of wound healing. Wound Repair Regen. 6, 531–542.

Sun, S., Wise, J., Cho, M., 2004. Human fibroblast migration in three-dimensional collagen gel in response to non-invasive electrical stimuli: I. Characterization of induced three-dimensional cell movement. Tissue Eng. 10, 1548–1557.

Suzuki, K., Saito, J., Yanai, R., Yamada, N., Chikama, T., Seki, K., Nishida, T., 2003. Cell-matrix and cell-cell interactions during corneal epithelial wound healing. Prog. Retin. Eye Res. 22, 113–133.

Teixeira, A.I., Abrams, G.A., Bertics, P.J., Murphy, C.J., Nealey, P.F., 2003. Epithelial contact guidance on well-defined micro- and nanostructured substrates. J. Cell. Sci. 116, 1881–1892.

Teixeira, A.I., Nealey, P.F., P.J., Murphy, C.J., 2004. Responses of human keratocytes to micro- and nanostructured substrates. J. Biomed. Mater. Res. 71A, 369–376.

Teixeira, A.I., McKie, G.A., Foley, J.D., Bertics, P.J., Nealey, P.F., Murphy, C.J., 2006. The effect of environmental factors on the response of human corneal epithelial cells to nanoscale substrate topography. Biomaterials 27, 3945–3954.

Vastrik, I., Eickholt, B.J., Walsh, F.S., Ridley, A., Doherty, P., 1999. Sema-3 induced growth cone collapse is mediated by rac 1 amino acids 17–32. Curr. Biol. 9, 991–994.

Vogelsgesang, M., Pautsch, A., Aktories, K., 2007. C3 exoenzymes, novel insights into structure and action of Rho-ADP-ribosylating toxins. Naunyn-Schmiedeberg's Arch. Pharmacol. 374, 347–360.

Walboomers, X.F., Croes, H.J.E., Ginsel, L.A., Jansen, J.A., 1998. Growth behaviour of fibroblasts on microgrooved polystyrene. Biomaterials 19, 1861–1868.

Wheeler, A.P., Wells, C.M., Smith, S.D., Vega, F.M., Henderson, R.B., Tybulewicz, V.L., Ridley, A.J., 2006. Rac1 and Rac2 regulate macrophage morphology but are not essential for migration. J. Cell. Sci. 119, 2749–2757.

Wojciak-Stothard, B., Curtis, A., Monoghan, W.M., MacDonald, K., Wilkinson, C., 1996. Guidance and activation of murine macrophages by nanometric scale topography. Exp. Cell Res. 223, 426–435.

Yamada, T., Ohoka, Y., Kogo, M., Inagaki, S., 2005. Physical and functional interaction of the lysophasphatidic acid receptors with PDZ domain-containing rho guanine nucleotide exchange factors (RhoGEFs). J. Biol. Chem. 280, 19358–19363.

Zhao, M., Agius-Fernandez, A., Forrester, J.V., McCaig, C.D., 1996a. Directed migration of corneal epithelial sheets in physiological electric fields. Investig. Ophthalmol. Vis. Sci. 37, 2548–2558.

Zhao, M., Agius-Fernandez, A., Forrester, J.V., McCaig, C.D., 1996b. Orientation and directed migration of cultured corneal epithelial cells in small electric fields are serum dependent. J. Cell. Sci. 109, 1405–1414.

Zhao, M., Dick, A., Forrester, J.V., McCaig, C.D., 1999. Electric field-directed cell motility involves up-regulated expression and asymmetric redistribution of the epidermal growth factor receptors and is enhanced by fibronectin and laminin. Mol. Biol. Cell 10, 1259–1276.

Zhao, M., Song, B., Pu, J., Forrester, J., McCaig, C.D., 2003. Direct visualisation of a stratified epithelium reveals that wounds heal by unified sliding of cell sheets. FASEB J. 17, 397–406.

Zhao, M., Song, B., Pu, J., Wada, T., Reid, B., Tai, G., Wang, F., Guo, A., Walczysko, P., Gu, Y., Sasaki, T., Suzuki, A., Forrester, J., Bourne, H., Devreotes, P.N., McCaig, C.D., Penninger, J.M., 2006. Electrical signals control wound healing through phosphatidylinositol-3-OH kinase-γ and PTEN. Nature 442, 457–460.